Proc. Indian Acad. Sci. (Chem. Sci.), Vol. 110, No. 3, June 1998, pp. 163–180.

Fundamental mechanisms of electronic and thermal ejection of material induced by pulsed laser beams

MELE A*[a], GIARDINI GUIDONI A[a], FLAMINI C[a], LATINI A[a], ORLANDO S[b], and TEGHIL R[c]
Dipartimento di Chimica, Università di Roma 'La Sapienza', Piazzale Aldo Moro 5, 00185 Roma, Italy
[b]Instituto Materiali Speciali-C N R, 85050 Tito Scalo (PZ), Italy
[c]Dipartimento di Chimica, Universita' della Basilicata, 85100 Potenza, Italy

Abstract. Laser ablation is a process which starts with absorption of the laser radiation followed by electronic excitation which may give rise to a thermal or electronic mechanism of particle ejection. The two types of processes have been extensively investigated experimentally and a great deal of phenomenological information have been gathered. Theoretical treatment provides, in the first case, a model based on thermodynamic properties of the solid surface and in the latter case refers to the electronic characteristics of the solid. The present brief overview reports experimental results fitting one or the other mechanism and summarizes the theories describing a thermal or a non-thermal process of laser ablation.

Keywords. Laser ablation; electronic and thermal mechanisms; desorption threshold; laser radiation; electron stimulated desorption.

1. Introduction

Numerous studies on laser ablation have provided important information on the phenomenology of the effects caused by a laser beam on a solid target [1–5]. The process has been compared with sputtering by ions or energetic electrons and similarly laser ablation causes removal of the surface material. The two types of processes differentiate for the energy absorption mechanism, which in the first case, is typically collisional while in the latter is electronic followed by vibrational excitation [6]. Laser ablation in a low-yield sputtering is also termed laser induced desorption. The energy deposition and its transformation in the process of laser ablation depends on the usual laser characteristics, listed in table 1, and on the target properties. The main effect in ablation of any solid surface is absorption of the laser radiation which depends on the laser light intensity.

Table 1. Laser characteristics

– Photon energy, laser wavelength.
– Pulse duration.
– Fluence or pulse energy per unit area F(J/cm^2).
– Intensity I, power per unit area (W/cm^2).
– Φ flux photon per unit area (cm^{-2}).

*For correspondence

Table 2. Grouping of metallic and non metallic solids. (Adapted from ref [7])

	Metallic solids III-V and II-VI semiconductors	Oxides, Perovskite Superconductors	Non metallic solids Alkali halides and Alkaline heart halides Calcogenides
Electron-lattice coupling strength	weak or zero (?) $\alpha = 0$–$0{\cdot}9$	Intermediate $\alpha = 0$–5–2	Strong $\alpha = 2$–4
Initial laser-solid interaction	delocalized lattice or delocalized vibration modes (electron-phonon coupling)	formation of polarons (excited electrons and associated lattice-strain field)	V_k centers to self-trapped excitons Non vertical transition
Relaxation time	from Drude theory time < 1 ps	time ~ 1 ps	Decay to F-center and H-center (vacancy-interstitial pair) time < 1 ps
Mechanism	Electronic (possible) Heating to vaporization	Electronic (important)	Electronic. Relaxation of STE into defect pairs impart kinetic energy to interstitial atoms.

The Beer's law for one, two or multiphoton excitation may be applied as follows,

$$I(x) = I \exp(\sigma_1 c_1 + \sigma_2 c_2 + \cdots + \sigma_n c_n)x,$$

where I_0 is the incident intensity, σ_n is n-photon absorption coefficient and x is the vertical direction to the surface.

Laser light with photon energy greater than the band gap is strongly absorbed. If hv is less than the Eg, band gap energy, the solid is transmissive. Laser absorption is followed by electronic excitation which may give rise to a thermal or electronic mechanism of particle ejection [7]. The borderline of these two mechanisms although it exists, is very difficult to define. A classification of the material according to their properties is provided in table 2 where metallic and non-metallic solids together with solids with intermediate properties are reported [7]. Table 2 summarizes this view, and refers and takes into account important solid properties and also the possible mechanisms of laser ablation. Solids have different electronic properties such as band gap energy, electron lattice coupling strength and crystal structure. Metals and alkali halides are the two extremes. III-V and II-VI group semiconductors, simple and mixed oxides, perovskite superconductors and calcogenides are substances which are grouped between the two extremes–metals and non-metals.

The early experiments on laser ablation, primarily in the IR, were conducted at very high laser intensity and fluence, with the ablated plume in thermal equilibrium [8,9]. Conversely to these experiments, lately it has been found that there are a large number of materials which may undergo a direct photochemical process of bond breaking by using UV and visible laser light sources [7,10–12]. The laser-target interaction is initially electronic and by relaxation tends to degrade to thermal on a subpicosecond time scale. The identification of the fundamental mechanism of electronic excitation and relaxation leading to ablation is a rather complex task, but so far a good deal of information of the nature of the mechanism has been obtained.

The observed pulsed laser ablation (PLA) phenomenology as seen, depends on one side, from the laser characteristics and on the other, from the thermodynamic and electronic properties of the solid target. Some explicit factors which have been found to affect the mechanism of PLA are reported in the following: the density of the electronic excitation depends on the band-gap energy and on the laser fluence so that both laser characteristics and material properties are involved; the electron-lattice coupling strength is a function of the ionicity; for laser photon energy $\ll$ band-gap, it should be possible to induce a direct multiphoton excitation into the conduction band and then heating of the lattice even in the case of excitation with fs pulses; the question of electronic processes in laser ablation requires the knowledge of the dynamics of energy deposition and relaxation following the laser pulse and lastly that the thermodynamic properties of the target are involved in the stage when electronic excitation degrades to heating the surface of the target.

2. Thermal process of pulsed laser ablation

It is believed that PLA from metal surfaces is largely due to a thermal process by melting and vaporization of the target with ejection of atoms, ions, electrons, and clusters [13]. The mechanism following initial electronic laser-solid interaction is termed normal vaporization. A sequence of events following the initial interaction between the laser beam and a solid metallic surface has been suggested. The initial effect of laser ablation of metal is the electron-phonon coupling, which is described by the constant g of the coupled equations for the electrons and of the lattice [14]. The laser light produces a high density of electronic excitation and the observed energy goes to delocalized lattice vibration modes. Diffusion of the moving electrons results in the ejection of the ions from the lattice before energy is thermalized ($\tau < 1$ ps). The assumption is that although the primary laser-surface interaction is mainly electronic, most of the deposited energy was rapidly converted to thermal energy. Three types of processes have been suggested, normal vaporization and normal boiling for $T \ll T_{tc}$ [15-16] and phase explosion for $T \cong 0{\cdot}9\ T_{tc}$ [17-20]. A phase diagram of a metal is reported in figure 1 [17]. This diagram represents the thermal trend of normal vaporization and superheating of a metal.

Many authors have treated the thermal process of laser ablation of metals [20-25]. The flux of particle emission is given by Hertz–Knudsen equation,

$$\text{flux} = \alpha p_o \left(\frac{1}{2\pi m k_B T}\right)^{1/2} \text{cm}^{-2}\,\text{s}^{-1}. \tag{1a}$$

Here, α is the condensation (or vaporization) coefficient, p_o is the equilibrium vapour pressure and m is the particle mass. With the assumption that the Clausius–Clapeyron equation can be applied to evaluate vapour pressure as a function of temperature, the velocity of surface recession in one dimension, i.e. the velocity of material removal by thermal heating of the surface is,

$$\frac{\partial x}{\partial t_{x=0}} \approx \alpha p_b \frac{m}{\rho}\left(\frac{1}{2\pi m k_B T}\right)^{1/2} \exp\left[\frac{\Delta H_v m}{k_B}\left(\frac{1}{T_b} - \frac{1}{T}\right)\right], \tag{1b}$$

where x is the direction normal to the target, p_b is the boiling pressure, ΔH_v is the heat of vaporization, ρ is the target mass density, and T_b is the boiling temperature.

The temperature at the target surface and the removal of material, due to the laser pulses, have been determined by solving the one-dimensional heat-diffusion equation using a finite difference method under particular boundary conditions assuming

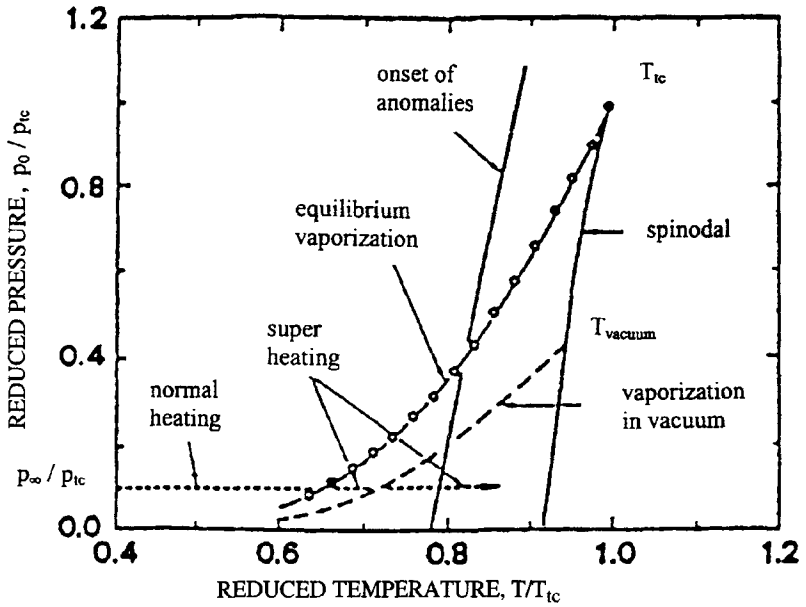

Figure 1. State diagram of a metal in the high-temperature region in the neighbourhood of T_{tc}. Equilibrium vaporization refers to experimental equilibrium vapor pressure for Cs. Vaporization in vacuum refers to a rapid heating in vacuum [17].

melting and vaporizaton in accordance to (4). The temperature at any point inside the target is controlled by the heat-diffusion equation,

$$c_p\rho\frac{\partial T(x,t)}{\partial t} = K\frac{\partial^2 T(x,t)}{\partial x^2} + v_r c_p \rho\frac{\partial T(x,t)}{\partial x} + S(x,t) + F(x,t)\delta(x - x_{int}), \quad (2)$$

where T, $c_p(T)$, $\rho(T)$, $K(T)$, v_r, and $S(x,t)$ are, respectively, temperature, specific heat, mass density, thermal conductivity, recession velocity as in (1), and the heat source. The term $F(x,t)$ in (2) takes into account the heat balance due to melting and solidification at the liquid-solid interface. δ is the Dirac delta function, x refers to the direction perpendicular to the plane of the target, t refers to time after the laser pulse, and x_{int} is the depth of the solid-liquid interface. Neglecting radiative loss from the target surface ($x = 0$), and the temperature dependence of c_p, ρ, and K, the following boundary conditions may be assumed,

$$T(x,t)_{x\to\infty} = T(x,t)_{t\to 0} = T_{amb}, \quad (3)$$

where T_{amb} is the ambient target temperature. The following heat balance at the target surface (more precisely: half a spatial step beneath the surface) may be now schematized for conditions of finite spatial and temporal steps as used in the calculations[24],

$$\textit{laser source} = \textit{conduction} + \textit{melting} + \textit{vaporization} + \textit{temperature change}, \quad (4a)$$

$$S(x,t)\frac{\Delta x}{2} = K\frac{T_0^i - T_1^i}{\Delta x} + (\Delta H_m + \Delta H_v)\rho v_r + c_p\rho\frac{\Delta x}{2}\frac{T_0^{i+1} - T_0^i}{\Delta t}, \quad (4b)$$

where i is the temporal index, and 0 and 1 are the spatial indices referred to the surface and to the first step, respectively.

The results of this treatment in the case of *Al* and *W* are reported in figure 2. The surface temperature, the recession velocity, and the crater depth as a function of time

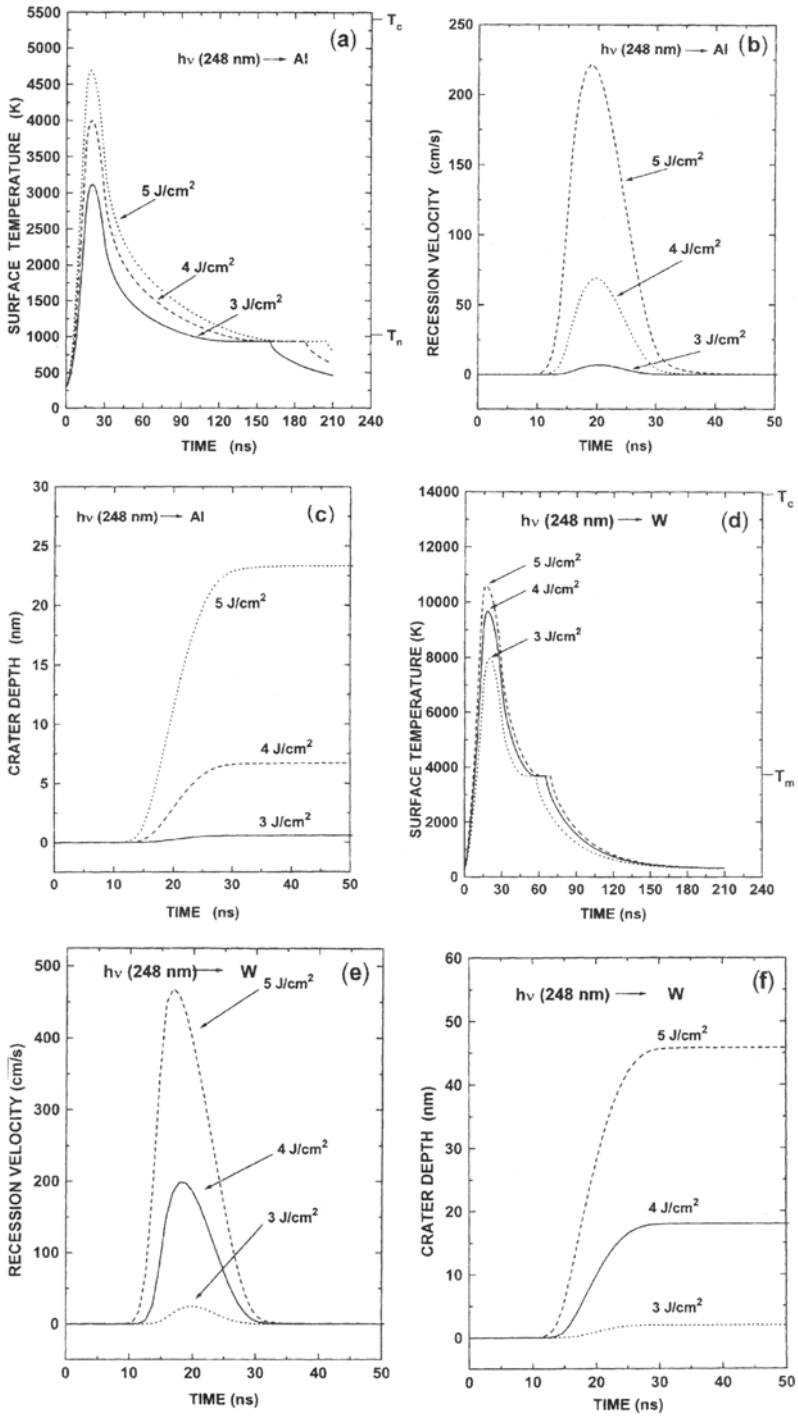

Figure 2. Aluminium sample, irradiated with a single pulse of a KrF laser, for four fluences **(a)** calculated surface temperature. The plateau corresponds to the melting temperature, **(b)** velocity of recession **(c)** crater depth. According to the recession velocity, the crater depth reaches the asymptotic value at the end of the laser pulse. In **(d)**, **(e)**, and **(f)** the correspondent calculations are for a tungsten sample.

have been calculated assuming a triangular shape for the laser pulse. These plots show the calculated trend for the two metals on the basis of their thermophysical properties as reported in table 3. For tungsten, surface temperature, recession velocity, and crater depth are calculated to be higher by a factor of 2 with respect to aluminium. As expected, it can be seen from the plots and this table that the main parameters affecting the thermal behaviour are ΔH_v, K and R. The higher these parameters, the smaller is the amount of material removed from the surface of the target. The calculated and the experimental values of the weight loss for an Al target are reported in figure 3. It should be noted that the significant discrepancy of the theory is based on an assumed equilibrium between the vaporization flux and the temperature of the target surface.

The previous discussion dealt with the thermal effects of the laser light on the surface. At this stage it may be interesting to look at what happens to the particles released and moving away from the solid target so as to get more information on the primary mechanism. The plot of figure 4a shows the velocity of expansion of the plume produced from an Al target. The flow velocity of the contact front (CF, i.e. the front edge of the total light emission) is given by Kelly and Miotello [6],

$$u_{CF} = \frac{2}{\gamma - 1} a_4, \tag{5a}$$

provided there is no ambient gas. Here $a_4 = (\gamma k_B T_4/m)^{1/2}$ is the sound speed and $\gamma = C_p/C_v$ is the heat-capacity ratio ($\gamma = 5/3$) for ground-state atoms). The corresponding reservoir energy, E_4, follows from the relation,

$$\frac{1}{2} m u_{CF}^2 = \frac{2m}{(\gamma-1)^2} a_4^2 = \frac{4\gamma}{3(\gamma-1)^2} E_4 \approx 5E_4. \tag{5b}$$

Table 3. Parameter values employed for the numerical analysis of the examined metals (ref.) [25].

	Al	W
T_m(K)	934	3680
T_b(K)	2790	5828
T_{tc}(K)	5410	13890
ΔH_m(J/kg)	396×10^3	192×10^3
ΔH_v(J/kg)	10500×10^3	4480×10^3
c_p(JK^{-1}kg^{-1})	940	133
K_{solid}(Js^{-1}m^{-1}K^{-1})	225	89·5
K_{liquid}(Js^{-1}m^{-1}K^{-1})	100	70·5
R	0·79	0·51
μ(m^{-1})	$5{\cdot}68 \times 10^7$	$9{\cdot}59 \times 10^7$

T_m = melting temperature, T_b = boiling temperature, T_{tc} = thermodynamic critical temperature, ΔH_m = latent heat of fusion at the melting temperature, ΔH_v = latent heat of vaporization at the boiling temperature appropriate to $p = 1$ atm, c_p = specific heat at constant pressure ($p = 1$ atm), K_{solid} = thermal conductivity of the solid at room temperature, K_{liquid} = thermal conductivity of the liquid at room temperature, R = reflection coefficient at $\lambda = 248$ nm, μ = absorption coefficient at $\lambda = 248$ nm.

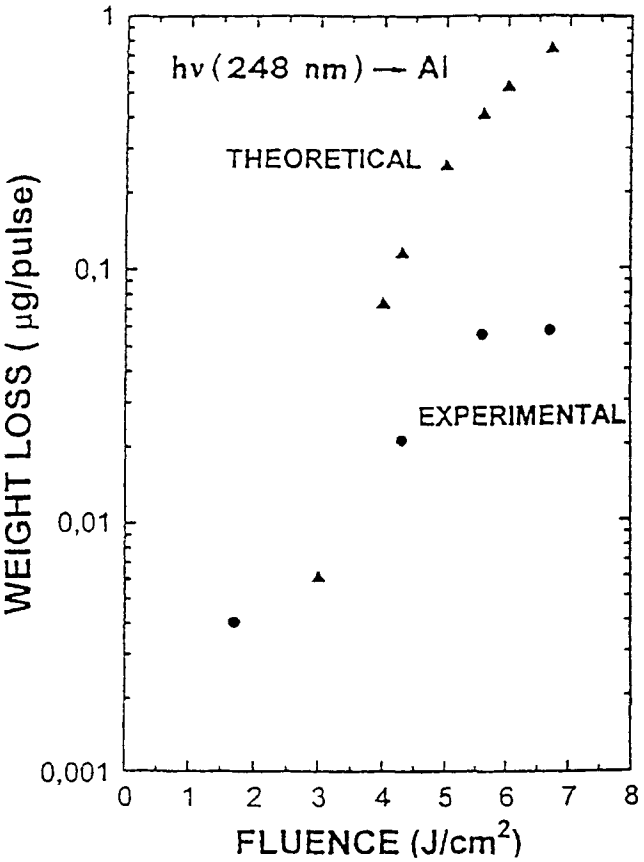

Figure 3. Experimental and calculated data of weight loss of an Al target, irradiated by a KrF laser (248 nm, $\tau = 30$ ns), as a function of fluence.

The plot of figure 4b shows that E_4 exceeds $3k_B T_{tc}/2$ to a certain extent and that a release mechanism involving normal vaporization by itself can be excluded.

The open questions which arise now are: what is the origin of high expansion velocities and energies of the particle released and why is there such a large discrepancy for the weight loss between theory and experiments. These questions may have more than one answer. It may be considered first that, by coupling the light frequency with the plasma frequency, a significant part of the incoming laser energy is transferred to the plasma and only a lesser amount is dissipated in the solid. The effect is to generate an opaque plasma such as to reduce the laser coupling to the surface. This transition can be attributed to an Inverse Bremmsstrahlung (IB) process where free electrons absorb energy [26-30]. At the end, the net balance is that the energetic electrons create more ion/electron pairs by collision. This results in the conversion of electronic energy to nuclear motion and thus the mean kinetic energy may exceed $3k_B T_{tc}/2$ ($1\,eV$ for $T_{tc} = 11600$ K). Incidentally, it is interesting to show the results obtained by fast photography of the plume by an intensified charge-coupled device (ICCD) camera. Figure 5 shows intensity density contours of the plume obtained from an Al target. Ionic species and neutrals have been identified by filtering the total emission by pass-band filters. It can be seen that the ionic species move on the front, while the

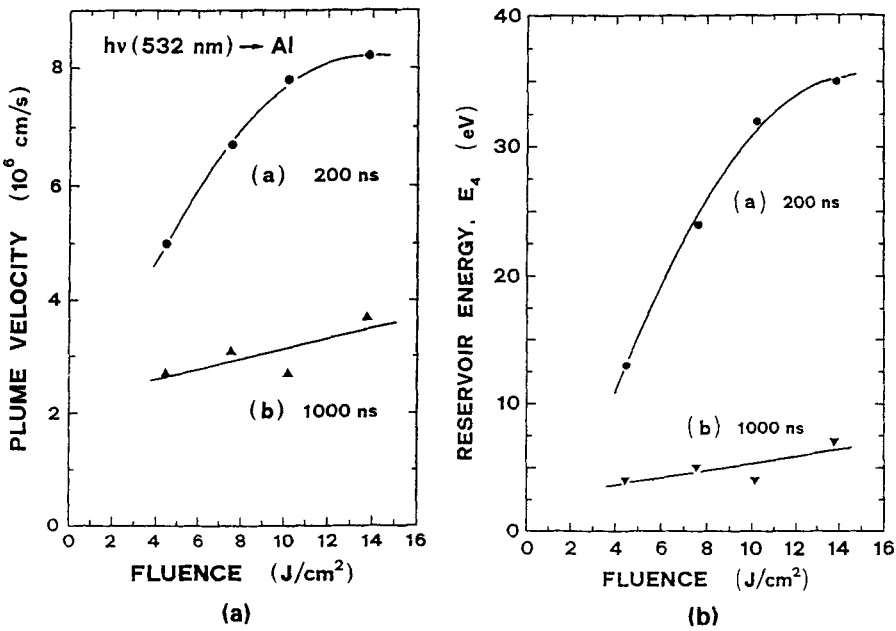

Figure 4. **(a)** Experimental mean velocity calculated according to equation (5a) for laser sputtered Al versus laser fluence. Nd-YAG ($\lambda = 532$ nm, $\tau = 6$ ns), **(b)** kinetic energy derived with 27 a.m.u. and $\gamma = 1{\cdot}25$ as for a monoatomic gas which is both ionized and excited.

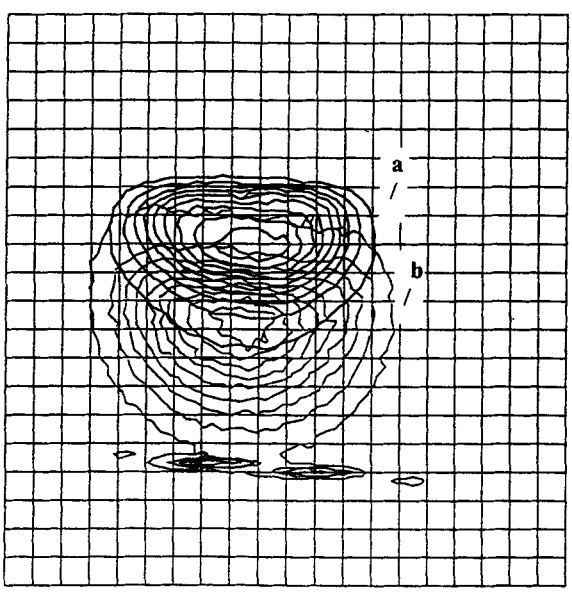

Figure 5. Composite intensity density contours of the plume obtained by an ICCD camera from an Al target, by filtering the plume at **(a)** $\lambda = 400$ nm and **(b)** $\lambda = 450$ nm. Grid step 2·5 mm.

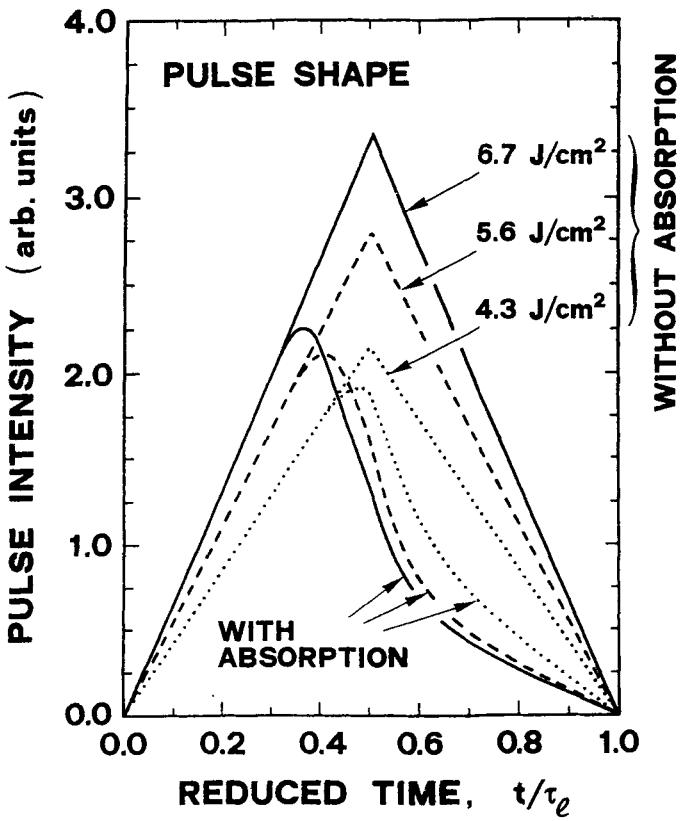

Figure 6. Triangular laser pulse corrected for absorption at three fluences. KrF laser ($\lambda = 248$ nm, $\tau_1 = 30$ ns).

neutral remains in the back part of the plume. The opacity of the plasma by IB may also explain the discrepancy observed between the weight loss calculated on a simple thermal model and the experimental values. This discrepancy may be corrected by introducing in the heat source term of the heat diffusion equation, a factor which depends exponentially on the crater depth $d(t)$: $S'(x,t) = S(x,t)e^{-cd(t)}$ as shown in figure 6, where $c = 3{\cdot}45{\cdot}10^{-8}\,\mathrm{m}^{-1}$ is an empirical parameter [31]. According to (4), the triangular laser pulse is modified. This shows the pulse shape as used in the calculation with and without absorption. From 20 to 46% of the pulse is absorbed in the range of fluence examined. In table 4 the experimental and the corrected calculated values of the weight loss are compared. Another reasonable answer may be obtained by considering that the Knudsen layer theory shows that a fraction of the emitted particles is backscattered toward the surface and is assumed to recondense. This is a well known phenomenon that has been reported in many experiments [6,32,33].

PLA from a copper disc by an excimer laser has been studied by laser induced fluorescence (LIF) [12]. The copper species (Cu^0, Cu^+ and Cu_2) have been detected in the plume at a distance between 0·5 and 2 cm from the target. Cu neutral appears to be produced by a simple vaporization mechanism regardless of whether laser ablation is with 193 or 351 nm radiation. The plot of log LIF intensity against fluence^{-1} demonstrates that the vapour density is proportional to experimental $(-1/T)$

Table 4. Calculated values from (2) and experimental data for a Al target ablation at various laser fluences. Kr-F laser ($\lambda = 248$ nm, $\tau = 30$ ns).

	Calculated								Experimental
Fluence (J/cm^2)	Maximum surface temperature (K)		Maximum surface recession (cm/s)		Crater depth depth per pulse (nm)		Weight loss (μmole/pulse)		Weight loss (μmole/pulse)
	(a)	(b)	(a)	(b)	(a)	(b)	(a)	(b)	
1·7	1809		$3*10^{-3}$		$2*10^{-4}$		$8*10^{-8}$		$0{\cdot}2*10^{-3}$
4·3	4233	3714	106	37	11	2	$4{\cdot}4*10^{-3}$	$1{\cdot}0*10^{-3}$	$0{\cdot}8*10^{-3}$
5·6	5016	3966	342	64	37	4	$14{\cdot}8*10^{-3}$	$1{\cdot}6*10^{-3}$	$2{\cdot}0*10^{-3}$
6·7	5505	4024	598	71	68	5	$27{\cdot}2*10^{-3}$	$1{\cdot}9*10^{-3}$	$2{\cdot}1*10^{-3}$

(**a**) without absorption
(**b**) with absorption

assuming $T \propto F$. There is a clear correlation between Cu^0 signal and vapour pressure thus justifying the view that Cu neutral is formed by a thermal mechanism with the surface at 3000 K. The velocity of the leading edge of Cu neutral near 1·2 J/cm² provides energies which increase gradually from 0·2 to 0·5 eV correspondingly, confirming a target temperature of about 3000 K [12].

3. Non thermal pulsed laser ablation

Laser induced desorption have similarities with electron stimulated desorption (ESD). In particular, ablation by UV lasers from some specific target material have shown that ESD and the laser ablation processes, which could be termed also photon stimulated desorption (PSD) [10,34], can both be explained on the basis of an electronic mechanism. An ESD mechanism has been developed by Menzel and Gomer [35], and in the same year by Redhead [36]. It was studied by the release of a gas from an adsorbed layer on a surface by an incident electron beam. The Menzel-Gomer-Redhead (MGR) model suggests that ions are produced by electronic excitation within the Franck–Condon region from a bonding state to a repulsive surface and move away from the surface gaining kinetic energy (figure 7). By neutralization, through an Auger process, neutrals can also escape from the surface depending on the kinetic energy acquired. Fragmentation of gas-phase molecules via Auger decay is reported [37], but this mechanism was proposed for the first time for a solid surface decomposition by Knotek and Feibelman [38]. A simple example of a normal decay is schematically shown here for K-ionized MgO molecule to various possible doubly-charged final states,

$$MgO + nh\nu \rightarrow [Mg^*O]^+ \quad \text{(a)}$$

$$[Mg^*O]^+ \rightarrow Mg^{2+} O + e^- \quad \text{(b)}$$

$$\rightarrow Mg^+ + O^+ + e^- \quad \text{(c)}$$

$$\rightarrow Mg^{2+} + O + e^- \quad \text{(d)}$$

$$\rightarrow Mg + O^{2+} + e^- \quad \text{(e)}$$

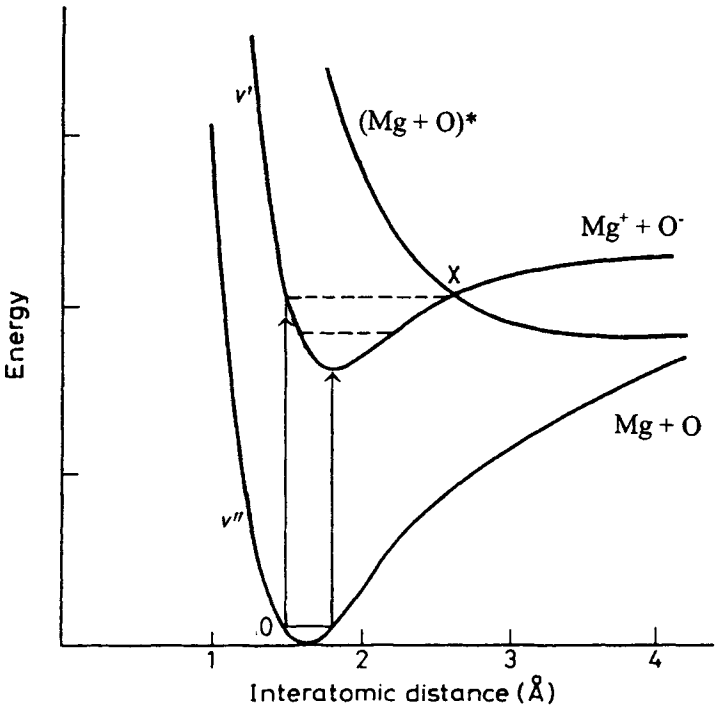

Figure 7. Potential-energy diagram for the bonding state M + O; ionic state $M^+ + O^-$, and the dissociative state. Vertical arrows show the Frank-Condon transitions.

where * = core hole in $K = 1s$ or $L_{2,3} = 2p$ levels. Processes (a) to (e) may also occur at MgO solid surface likely favoured by a defective structure.

For this model the theoretical threshold for desorption is typically predicted to be low. This is because the excitation energy between the O(2p) states and the (3sp) unoccupied states on MgO is about 10–15 eV. KF presents evidence for a fundamentally new model for ESD, based on Auger decay of core hole electronic excitation-ionization process. This model indicates that the ejection occurs through coulombic repulsion and explains why the threshold for ESD of positive ions from certain *d*-band metal oxide correlate in energy with the ionization potential of the highest lying atomic core levels. An energy diagram was constructed to calculate the maximum energy available to a desorbed O neutral or O^+ ion from a TiO_2 surface. The argument has been tested by looking at the ESD when other species are adsorbed on a metal oxide surface. By measuring low-energy electron loss spectroscopy (LEELS) and desorption yield versus incident electron energy, a correspondence between core-hole excitation and desorption threshold has been found. It should be noted that desorption occurs from oxides such as TiO_2, V_2O_5 and WO_3 where no valence electrons are left on the metal, while for NiO and Cr_2O_3 where there are valence electrons left on the metal atom, no desorption was observed. In the first case, the Auger decay is intratomic and thus rapid while in the latter there is an interatomic decay that is quite slow.

A schematic diagram is reported for the general case of a metal oxide (MO) which is considered to be 100% ionic. The scheme shows the Auger decay of shallow core

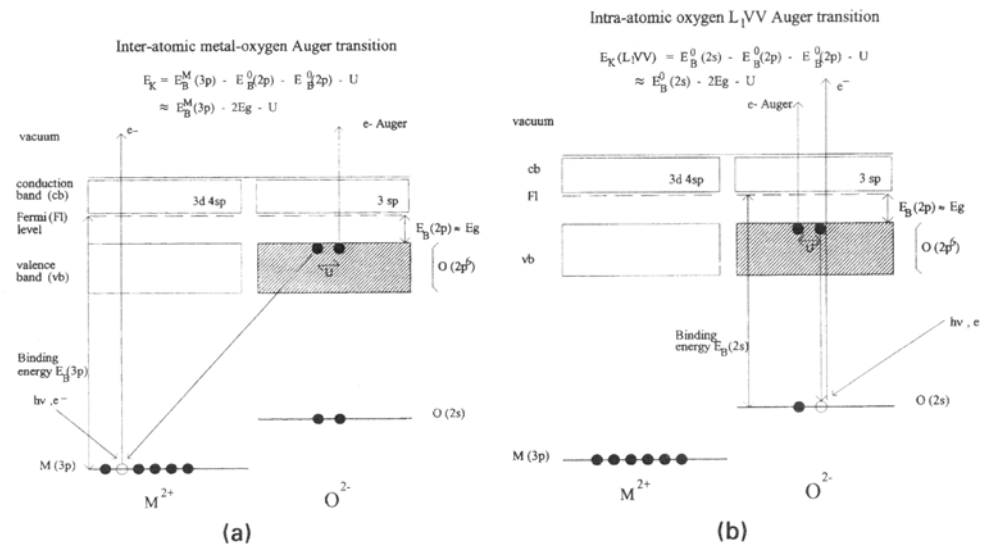

Figure 8. (**a**) Schematic of interatomic and (**b**) intratomic Auger transition for a model MO metal oxide (*n*-type). The energetic balance to calculate the kinetic energy of the escaping Auger electron is reported in the figure for the two cases.

levels created on the metal atom (figure 8a) and the O atom (figure 8b) by photon or electronic bombarding of the metal oxide target. Two fundamental processes are reported. The interatomic metal oxide Auger transition is shown in figure 8a with the relative energy involved. It can be seen that in the final state of the transition, a neutral O atom or even a positive O^+ ion (in the case of partially covalent MO bond) can be ejected. The intratomic oxygen LVV Auger transition of figure 8b indicates how to get to the same result starting from a O(2s) core level. It should be considered that the emission of positive or neutral O atoms makes it possible for the species to escape with significant kinetic energy from the solid surface. If the Auger electron remains trapped in the solid at the Fermi level, its energy (E_k see figure 8) is available and may be transferred to the ejected atom as desorption kinetic energy. The local Madelung potential at the oxygen sites typically of the order of 20–30 eV [39] is not effective anymore. This scheme does not involve the metal ejection. However the effect of the photoinduced desorption of the anion is such that the local structure at the cation sites is strongly strained. The creation of a wide number of vacancies could induce a drastic lowering of the local Madelung potential at the cation sites, thus affecting their ejection.

The mechanism of electronic excitation (either valence or core states) has been discussed in terms of the solid state properties of the target, semiconductors, oxide and alkali halides. Laser produced sputtering of non thermal origin involves excitation or ionization and assumes the formation of *sites* in the bulk or on the surface for localization of the energy which is converted to KE of atoms being emitted. The process of defect formation is initiated by the creation of electron-hole pairs or excitons followed by the formation of self trapped exciton (STE) [40–44]. In alkali halide the STE may be viewed as an electron bound by a coulombic field to alkali ions and hole which occupies an orbital of a molecular ion (X_2^-) (STE). In the colour centre terminology, self trapped holes (STH) are called V_K centres. A V_k centre is formed when a hole is trapped

by a pair of negative ions, and resembles a negative halogen molecular ion (X_2^-). Thus the self trapped exciton is generated when a self trapped hole (STH) (V_K) captures an electron. This state is referred to as [V_K e] or [X_2^{2-}] or STE i.e. a recombination of an electron with STH. A schematic of the various structural forms by photon lattice coupling are reported in figure 9 (a–d).

Studies on the creation of defects, STE, e-h pairs, as well as structural changes by ultraviolet plasma or laser irradiation of various systems have been reported and it is not the object of this brief review of electronic processes of laser ablation-desorption. These structures make possible the identification of localized sites characterizing the nature of the mechanism which is very important from a fundamental point of view but also for the various applications of laser ablation. Non thermal sputtering involves electronic excitation in the bulk valence bands or in surface defects. Self trapping of an exciton can satisfy the condition for formation of MGR-type adiabatic potential energy surface.

A large number of experiments showing direct evidence of ablation (desorption) by a non-thermal mechanism have been carried out. A few examples of ablation of alkali halides, semiconductors, oxides, and generally compounds with intermediate or very strong electron lattice coupling strength will be reported in the following.

The existence of a typical threshold energy density seems to be an important effect of the surface or of the bulk structure on the electronic mechanism of laser sputtering. Two laser techniques were used to probe the plume produced from insulating material with major reference to sapphire (Al_2O_3) with 248 nm pulses[45]. The first technique measures the free electron density using a Michelson interferometer while the second, measures by the laser induced fluorescence, the number density and energy distributions in the plasma when etching the material target. The plots of figure 10 show the results of these experiments and indicate a correlation between the data of the two types of experiments as a function of fluence. Further, time resolved experiments confirm the correlation between the plasma density and optical emission. The main result with sapphire and other materials is a clear evidence of the threshold from observation of etching of the surface and of the measurements reported in figure 10 both of which rule out a thermal mechanism of material removal and suggests a role of electronic excitation.

The velocity distribution peaks of AlO and Al from ablation of a sapphire target were measured by LIF time-of-flight spectroscopy[11]. The translational energy was evaluated to be in the range from 4 eV to 20 eV for a fluence from near the threshold up to 3 J/cm^2. These values are very high corresponding well above the critical temperature ($T_{ic} \approx 10000$ K). But for AlO the vibrational and rotational energies were smaller corresponding to a temperature of 500–600 K. This inequality $E_{trans} \gg E_{rot}$ is an explicit indication that the laser ablation could not be interpreted with normal vaporization but more likely with an electronic ablation mechanism.

Tentatively it may be suggested that a partial absorption of the laser radiation as discussed above by the plasma through an IB process could account for both the low surface temperature of the target and for the higher velocity of Al with respect to AlO. A selective absorption may produce an acceleration of the Al component which travel on the front edge.

Laser induced desorption of particles from sapphire (α Al_2O_3) surface has been recently reinvestigated by time-of-flight mass spectrometry and discussed with the aid of the results obtained by monitoring electronic and atomic structure of the surface by standard electron spectroscopy[46]. Above the ablation threshold, aluminium and

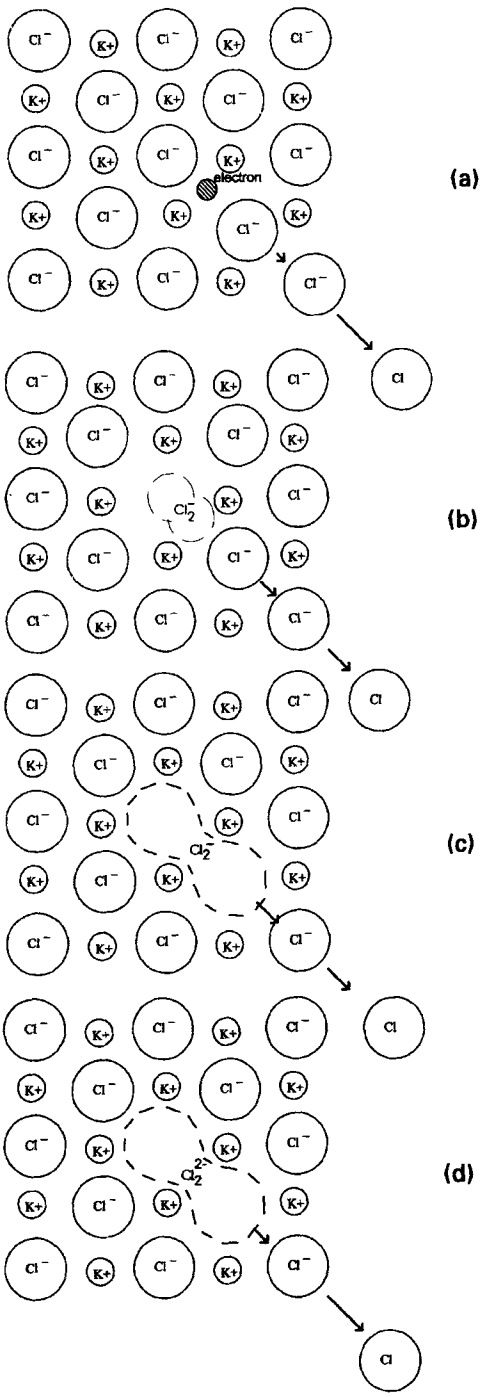

Figure 9. Structures where valence electrons lead to a localized strain in the lattice and the carrier is immobilized by the lattice field in a crystal of KCl. (**a**) Formation of a polaron, the electron is in a deformable lattice, (**b**) H centre is an interstitial ion bound to a lattice anion; (**c**) V_K or self trapped hole (STH) centre formed when a hole is trapped by 2 anion vacancy, (**d**) self trapped exciton formed when a STH captures an electron.

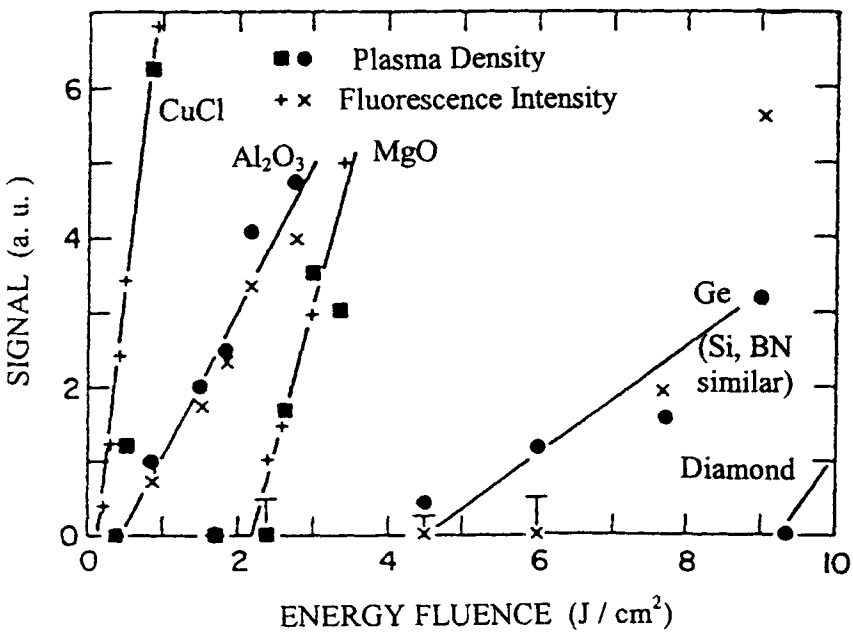

Figure 10. Threshold fluences for particle emission from CuCl, Al_2O_3, MgO, Ge and diamond for laser pulses from a 248 nm KrF excimer laser ($\tau = 20$ ns), measured from free electron density in the plume and by using laser induced fluorescence for optical emission (See reference [11].)

oxygen neutral particles and their combination were laser desorbed confirming previous findings [11]. Al ions were desorbed below the ablation threshold with mean kinetic energy as high as 7·7 eV. The measured time-of-flight distribution has been fit with a Maxwell–Boltzmann distribution and is independent from the laser fluence and from laser wavelength (355 nm or 1064 nm). These results strongly support the view that the desorption proceeds via an electronic. The process is described by the MGR model. The role of surface electronic structure is also reported. It is shown that the order of photon absorption process may be reduced by the presence of band-gap states such as seen in the energy loss spectrum. The unlikely photon absorption of six photons at 1064 nm wavelength could be strongly reduced at a lower order as for 355 nm referring to the presence of band-gap states such as seen in the energy loss (EL) spectrum [46]. A schematic representation of a possible desorption induced by electronic transitions (DIET) mechanism, for Al ions from sapphire, shows two potential-energy curves for the aluminium-sapphire surface interaction for the ground state and excited state as a function of aluminium atom surface separation. The electronic and atomic structures of the surface were affected by the photon absorption as observed by the change of the characteristics as shown by the spectroscopic technique used [46].

The Ga neutral yield produced by irradiation of GaP (1 1 0) surfaces by 28 ns laser pulses was studied at two different fluences 1·0 J/cm^2 and 1·2 J/cm^2. In the first case, the sputtering yield decreases rapidly at the beginning of the irradiation and remains constant for about 8000 laser shots. By increasing the fluence to 1·2 J/cm^2 an increase of

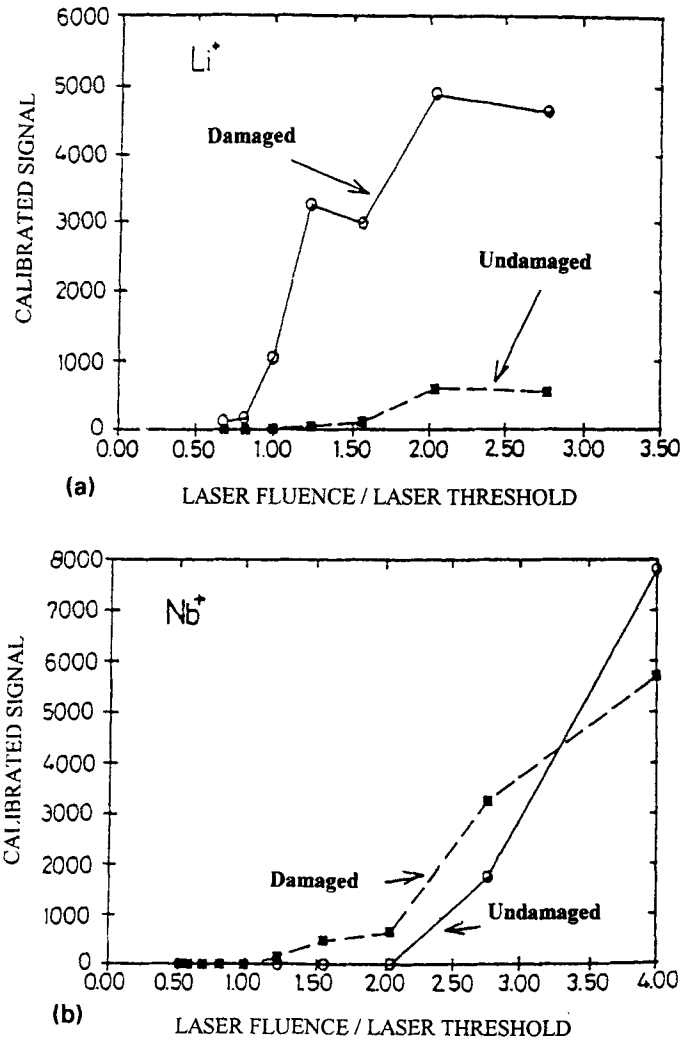

Figure 11. Sputtering yield for Li^+ and Nb^+ from $LiNbO_3$ surface by irradiating with laser pulses from a XeCl excimer laser (308 nm) for damaged and undamaged samples.

the yield was measured. This strongly suggests the role of the surface perfection of the sputtering yield. This is an explicit effect due to the surface conditions and to the fluence. Low laser fluence creates a perfect surface which becomes less perfect by increasing the fluence by only 20% [42].

The role of the surface on the sputtering yield has also been shown for Li^+ and Nb^+ ejection from a ferroelectric insulator $LiNbO_3$ by pulsed laser sputtering [10]. A significant difference exists between desorbed Li^+ and Nb^+ depending on the observed surface modification of the sample after laser irradiation. These results are illustrated in figure 11. The Nb^+ threshold is almost the same for the undamaged and the damaged sample and the hypothesis is that a thermal mechanism occurs in either cases. Li^+ emission is considered to be non thermal because of the large difference of the

sputtering yield depending on whether or not the irradiated spot had previously received a significant number of laser shots.

4. Conclusions

The present work has shown some experimental results on the laser-solid interaction and has discussed laser ablation (sputtering) in the light of the mechanisms involved to produce material ejection from solid target. However, this brief review of the experimental and theoretical features of the laser plasma plume cannot be exhaustive. A purely thermal approach failed to provide an agreement between theory and experiments. The phenomenology is quite complex and the many approximations for theoretical treatment were not adequate. Experimentally it has been found that the parameters which affect laser ablation are difficult to disentangle. The complexity of the problem makes the theoretical treatment a difficult task. Solutions are possible only by simplified models. A more sophisticated approach based on the electronic excitation and ion production in the target, in terms of the dynamics of the events based on electronic and thermodynamic properties of the material is to be developed. MGR and KF models together with emphasis to bond breaking of bonded atoms around structural defects seem to be more satisfactory by including a structural picture of the solid.

Acknowledgments

This work was financially supported by Italian Consiglio Nazionale delle Ricerche under "Progetto strategico materiali innovativi". The authors acknowledge G Moretti for helpful discussions in the preparation of this work.

References

1. Mele A, Giardini Guidoni A and Teghil R 1994 *La Chimica e l'Industria (in English)* **76** 120
2. Athwal I S, Mele A and Ogryzlo A 1992 *Diamond Relat. Mater.* **1** 731
3. Giardini Guidoni A, Mele A, Di Palma T M, Flamini C, Orlando S and Teghil R 1997 *Thin Solid Films* **295** 77
4. Mele A, Giardini A and Teghil R 1996 In *NATO ASI Frontiers in nanoscale science of micron/submicron devices* (eds) A P Jauho and E V Buzaneva (The Netherlands: Kluwer Academic Press) p 67
5. Ferro D, Gambardella U, Marotta V, Martino R, Morone A, Orlando S and Parisi G P 1994 *Appl. Surf. Sci.* **79/80** 455
6. Kelly R and Miotello A 1994 In *Pulsed laser deposition of thin films* (eds) D B Chrisey and G K Hubler (New York: John Wiley) p 55
7. Haglund R F and Kelly R 1992 *Mat. Fys. Medd. K. Dan. Vidensk. Selsk.* **43** 526
8. Feldmann D, Katzner J, Laukemper J, Macrobert S and Welge K H 1987 *Appl. Phys.* **B44** 81
9. Kuper S and Stuke M 1987 *Appl. Phys.* **B44** 199
10. Nakai Y, Hattori K, Okano A and Itoh N 1991 *Nucl. Instrum. Methods* **B58** 452
11. Dreyfus R W, Kelly R and Walkup R E 1986a *Appl. Phys. Lett.* **49** 1479
12. Dreyfus R W 1991 *J. Appl. Phys.* **69** 1721
13. Mele A, Consalvo D, Stranges D, Giardini Guidoni A and Teghil R 1990 *Int. J. Mass Spectrom. Ion Phys. Proc.* **95** 359
14. Anisimov S I, Kapeliovich B L and Perel'man T L 1975 *Sov. Phys. JEPT* **39** 375
15. Kelly R and Miotello A 1996 *Appl. Surf. Sci.* **96–98** 205
16. Miotello A and Kelly R 1995 *Appl. Phys. Lett.* **67** 3535
17. Martynyuk M M 1974 *Sov. Phys. Tech. Phys. (Engl. Transl.)* **19** 793
18. Fucke W and Seydel U 1980 *High Temp. High Pressures* **12** 419

19. Seydel U and Fucke W 1978 *J. Phys. F.* **8** 157
20. Dawson J, Kaw P and Green B 1969 *Phys. Fluids* **12** 875
21. Ready J F 1971 *Effects of high power laser radiation* (New York: Academic Press) p 1
22. Peterlongo A, Miotello A and Kelly R 1994 *Phys. Rev.* **E50** 4716
23. Pound G M 1972 *J. Phys. Chem. Ref. Data* **1** 135
24. Flamini C 1996 thesis, University of Rome 'La Sapienza' Italy
25. Mele A, Giardini Guidoni A, Kelly R, Flamini C and Orlando S 1997 *Appl. Surf. Sci.* **109–110** 584
26. Ljuboje Z, Konjevic N, Popovic M and Cirkovic Lj 1987 *Opt. Commun.* **63** 248
27. Bakos J S, Ignacz P N, Szigeti J and Kovacs J 1987 *Appl. Phys. Lett.* **51** 734
28. Rothenberg J E and Koren G 1984 *Appl. Phys. Lett.* **44** 664
29. Holtgen N, Horneff P, Kreutz E W and Treusch H G 1986 *Rev. Roum. Phys. Tome* **31** 1073
30. Ramsden S A and Savic P 1964 *Nature (London)* **203** 1217
31. Svendsen W, Ellegard O and Schou J 1996 *Appl. Phys.* **A63** 246
32. Miotello A, Kelly R, Braren B and Otis C E 1992 *Appl. Phys. Lett.* **61** 2784
33. Kelly R, Miotello A, Braren B and Otis C E 1992 *Appl. Phys. Lett.* **60** 2980
34. Helvajian H and Welle R 1989 *J. Chem. Phys.* **91** 2616
35. Menzel D and Gomer R 1964 *J. Chem. Phys.* **41** 3311
36. Redhead P A 1964 *Can. J. Phys.* **42** 886
37. Kay R B, Van der Leeuw Ph E and Van der Wiel M J 1977 *J. Phys.* **B10** 2521
38. Knotek M L and Feibelman P J 1978 *Phys. Rev. Lett.* **40** 964
39. Broughton J Q and Bagus B S 1980 *J. Electron Spectrosc.* **21** 283
40. Mott N F and Garney R W 1964 *Electronic process in ionic crystals* (New York: Dover)
41. Williams R T and Song S J 1990 *J. Phys. Chem. Solids* **51** 679
42. Itoh N 1982 *Adv. Phys.* **31** 491
43. Itoh N 1985 *Cryst. Lattice Defects Amorph. Mater.* **12** 103
44. Itoh N and Tanimura K 1990 *J. Phys. Chem. Solids* **51** 717
45. Dreyfus R W, Walkup R E and Kelly R 1986b *Radiat. Eff.* **99** 199
46. Schildbach M A and Hamza A V 1992 *Phys. Rev.* **B45** 6197